Supporting Information

Perovskite quantum dots for Lewis acid-base interaction and interface engineering in lithium-metal batteries

Yuchen Wang[#], Wen Li[#], Zhong Xu, Yanting Xie, Yihan Wang, Haibo Zhao, Junfeng Huang, Weiqing Yang, Haitao Zhang[*]

Key Laboratory of Advanced Technologies of Materials, Ministry of Education,

School of Materials Science and Engineering, Southwest Jiaotong University,

Chengdu 610031, China

[#]These authors contributed equally to this work.

*Corresponding author: haitaozhang@swjtu.edu.cn (H. T. Z.)

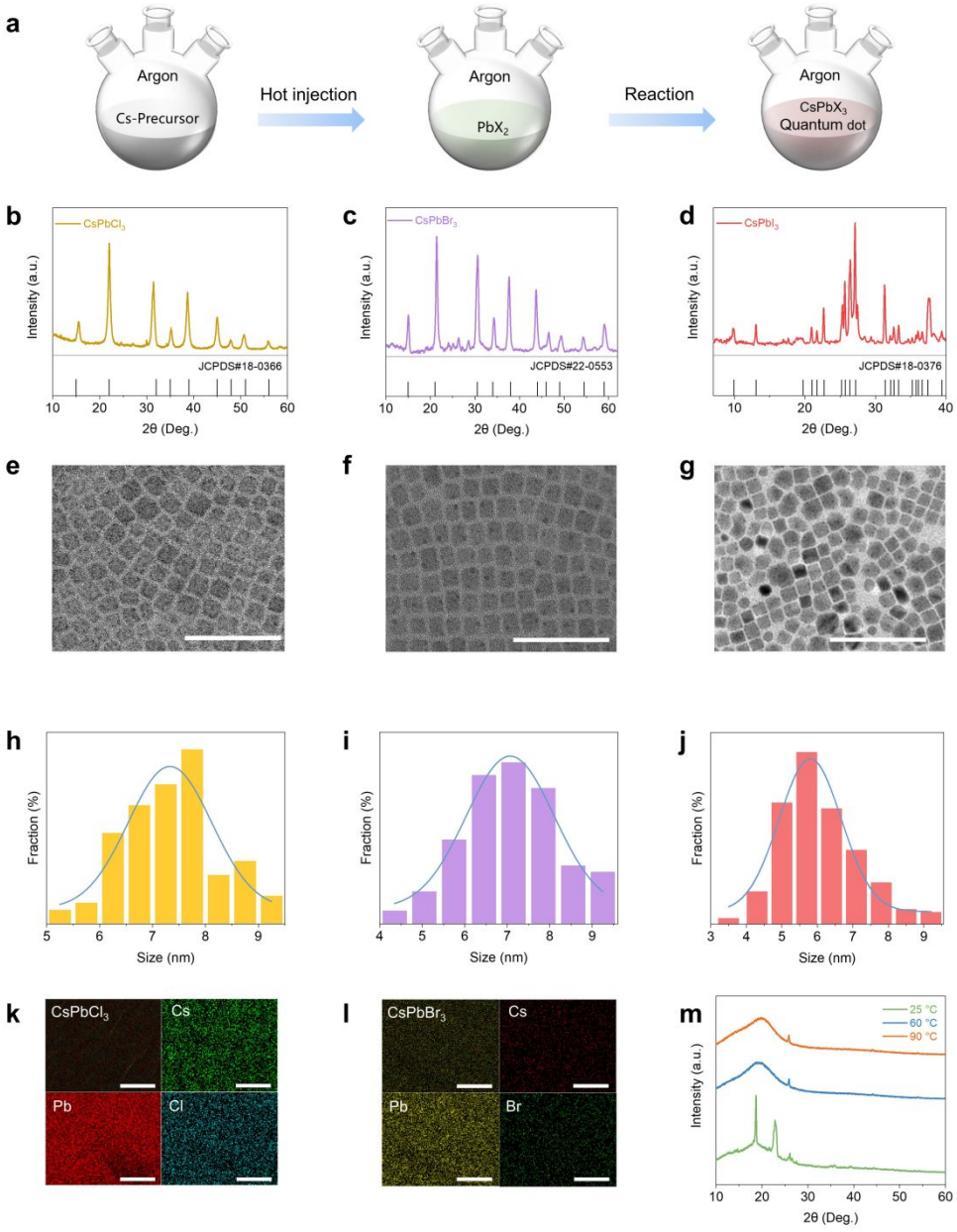

Figure S1. a, Detailed synthetic process of $CsPbX_3$ PQDs. **b, c, d,** XRD patterns of (**b**) $CsPbCl_3$, (**c**) $CsPbBr_3$ and (**d**) $CsPbI_3$ PQDs. **e, f, g,** TEM images of (**e**) $CsPbCl_3$, (**f**) $CsPbBr_3$ and (**g**) $CsPbI_3$ PQDs. **h, i, j,** Size distribution of (**h**) $CsPbCl_3$, (**i**) $CsPbBr_3$ and (**j**) $CsPbI_3$ PQD particles with a normal distribution. **k, l,** EDX elemental analysis of (**k**) PEO-$CsPbCl_3$ and (**l**) PEO-$CsPbBr_3$ SSEs. **m,** XRD patterns of PEO-$CsPbI_3$ SSEs at 25 °C, 60 °C and 90 °C. Scale bars: 50 nm in **e, f and g**, and 25 μm in **k** and **l**.

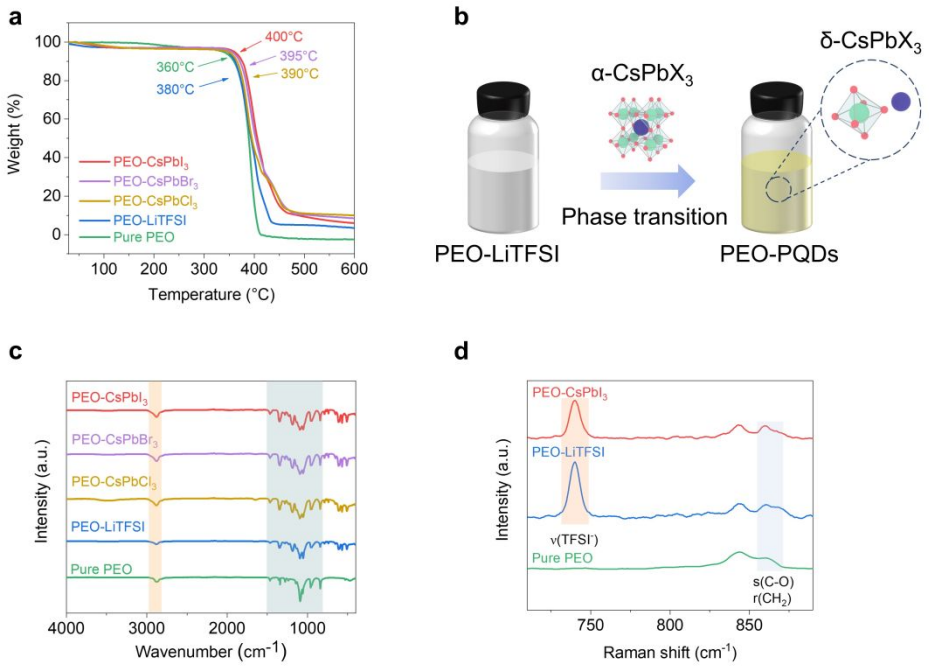

Figure S2. a, TGA curves of the thermal property of SSEs. **b,** The phase transition process of $CsPbX_3$ PQDs. **c,** FTIR spectra of pure PEO, PEO-LiTFSI, and PEO-$CsPbX_3$ SSEs at 4000-400 cm^{-1}. **d,** Raman spectra of pure PEO, PEO-LiTFSI, and PEO-$CsPbI_3$ SSEs at 710-890 cm^{-1}.

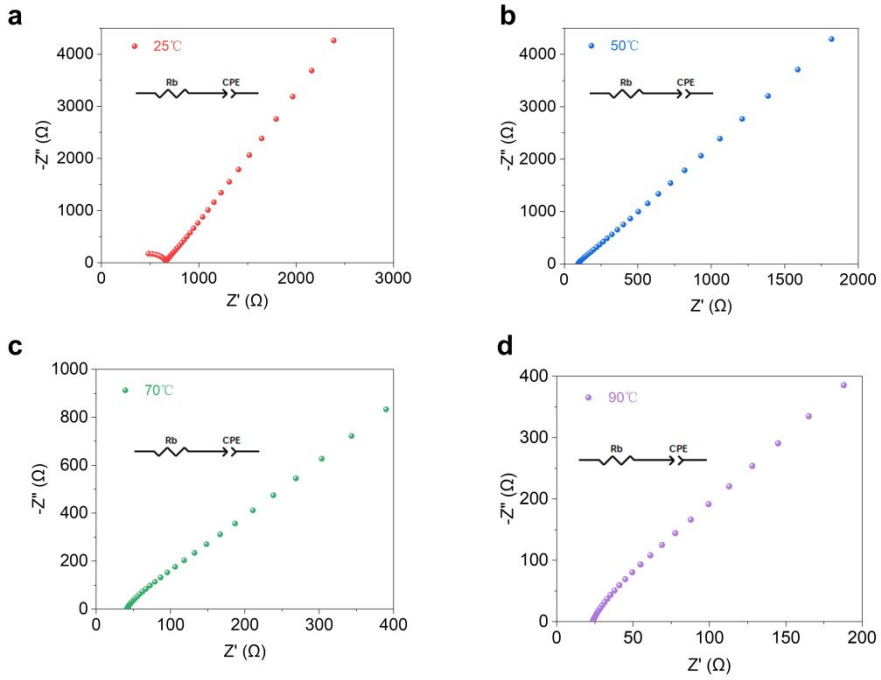

Figure S3. a, b, c, d, Nyquist plots of PEO-$CsPbI_3$ SSEs at (**a**)25 °C, (**b**)50 °C, (**c**)70 °C, (**d**)90 °C.

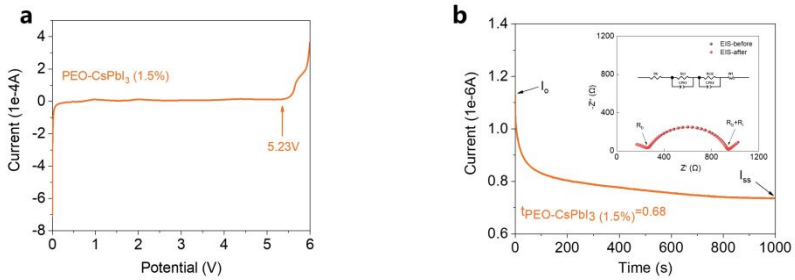

Figure S4. a, Electrochemical stability windows of 1.5% doped PEO-$CsPbI_3$ SSE. **b,** Lithium-ion transference number of 1.5% doped PEO-$CsPbI_3$ SSE.

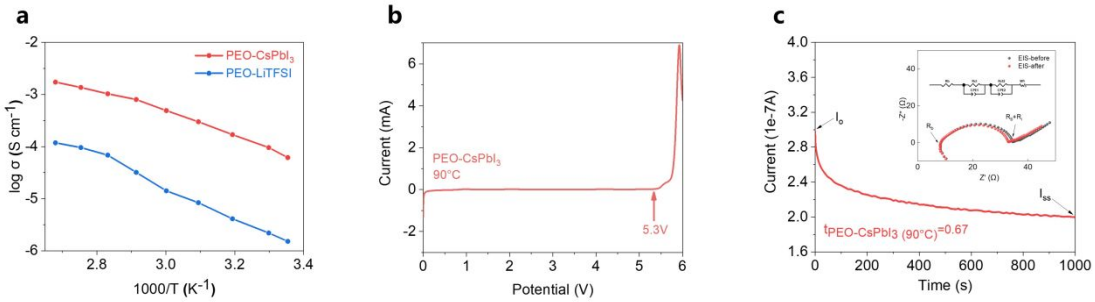

Figure S5. a, Arrhenius plots of ionic conductivity of PEO-$CsPbI_3$ and PEO-LiTFSI SSEs. **b,** Electrochemical stability window of PEO-$CsPbI_3$ SSE at 90 °C. **c,** Lithium-ion transference number of PEO-$CsPbI_3$ SSE at 90 °C.

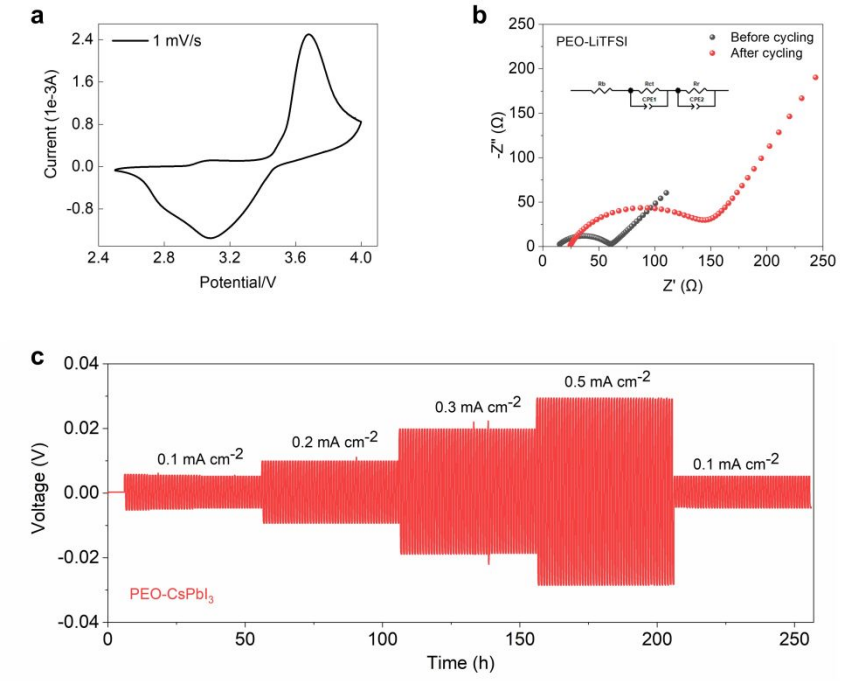

Figure S6. a, Cycling voltammetry curves of LMBs with PEO-$CsPbI_3$ SSEs at the rate of 1 mV s^{-1} at 90°C, indicating the charging and discharging plateau is around 3.6 and 3.1 V, respectively. **b,** EIS spectra of Li/PEO-LiTFSI/LFP LMBs before and after 100 cycles at 0.1C at 90 ° C. Inset: the equivalent circuit of the impedance spectra. **c,** Galvanostatic cycling curves of Li/PEO-$CsPbI_3$/Li batteries at various current densities at 90°C.

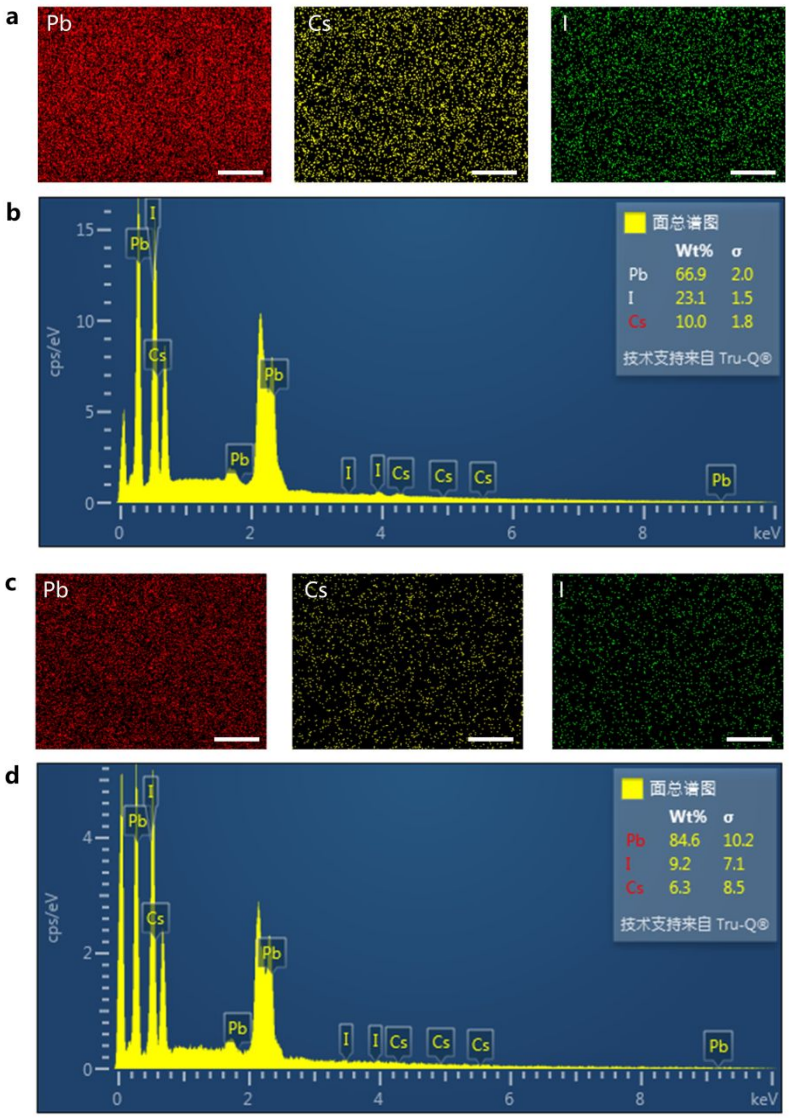

Figure S7. a, EDX elemental analysis of PEO-$CsPbI_3$ SSEs before battery test. **b,** element mass percentages of PEO-$CsPbI_3$ SSEs before battery test. **c,** EDX elemental analysis of PEO-$CsPbI_3$ SSEs after battery test. **d,** element mass percentages of PEO-$CsPbI_3$ SSEs after battery test.

Table S1. Thermal properties of SSEs.

Sample	T_g (°C)	T_m (°C)	ΔH_m (J g^{-1})	χ_c (%)
Pure PEO	-56.5	62.62	156.69	77.19
PEO-LiTFSI	-40.85	49.46	45.68	22.50
PEO-$CsPbCl_3$	-48.24	44.45	38.61	19.02
PEO-$CsPbBr_3$	-46.31	43.93	36.43	17.95
PEO-$CsPbI_3$	-50.03	42.13	33.14	16.32

Where T_g, T_m, ΔH_m and χ_c represent the glass transition temperature, melting point, melting enthalpy and crystallinity, respectively.

Table S2. FTIR peaks and assignments for SSEs.

Peak Assignment	Wavenumber/cm^{-1}				
	Pure PEO	PEO-LiTFSI	PEO-$CsPbCl_3$	PEO-$CsPbBr_3$	PEO-$CsPbI_3$
$\gamma(CH_2)_a$	841	842	842	842	842
$\gamma(CH_2)_s$	961	959	959	959	959
$\omega(CH_2)_a$	1360	1351	1351	1351	1351
$\nu(COC)_s$	1059	1056	1058	1057	1057
$\nu(COC)_a$	1092	1094	1091	1091	1091
$\nu(CF_3)_s$		1185	1186	1186	1187
$\nu(OH)$	3460	3460	3460	3460	3460

Table S3. Raman peaks and assignments for SSEs.

Peak Assignment	Wavenumber/cm^{-1}		
	Pure PEO	PEO-LiTFSI	PEO-$CsPbI_3$
r(CF_3)		275	277
r(SO_2)		311, 326, 342	309, 325, 338
b(COC)	362	362	362
v($TFSI^-$)		740	740
s(C-O) r(CH_2)	860	860	860
t(CH_2)	1280	1280	1280
s(CF_3)		1242	1240
s(C-C) s(C-O)	1140	1140	1140
s(SO_2)		1136	1140